Combining Instantaneous Temperature Measurements and CFD for Analysis of Fuel Impingement on the DISI Engine Piston Top

Kukwon Cho[1]
Ronald O. Grover, Jr.[2]
Dennis Assanis
Zoran Filipi

Department of Mechanical Engineering,
University of Michigan,
Ann Arbor, MI 48109

Gerald Szekely
Paul Najt
Rod Rask

General Motors Research and Development,
Warren, MI 48090-9055

A two-pronged experimental and computational study was conducted to explore the formation, transport, and vaporization of a wall film located at the piston surface within a four-valve, pent-roof, direct-injection spark-ignition engine, with the fuel injector located between the two intake valves. Negative temperature swings were observed at three piston locations during early injection, thus confirming the ability of fast-response thermocouples to capture the effects of impingement and heat loss associated with fuel film evaporation. Computational fluid dynamics (CFD) simulation results indicated that the fuel film evaporation process is extremely fast under conditions present during intake. Hence, the heat loss measured on the surface can be directly tied to the heating of the fuel film and its complete evaporation, with the wetted area estimated based on CFD predictions. This finding is critical for estimating the local fuel film thickness from measured heat loss. The simulated fuel film thickness and transport corroborated well temporally and spatially with measurements at thermocouple locations directly in the path of the spray, thus validating the spray and impingement models. Under the strategies tested, up to 23% of fuel injected impinges upon the piston and creates a fuel film with thickness of up to 1.2 μm. In summary, the study demonstrates the usefulness of heat flux measurements to quantitatively characterize the fuel film on the piston top and allows for validation of the CFD code. [DOI: 10.1115/1.4000293]

1 Introduction

The increasing emphasis on achieving substantial improvements in vehicle fuel economy calls for new engine concepts, providing improved efficiency, while complying with future stringent emission requirements. The fuel efficiency of the direct-injection (DI) diesel engine is superior to that of the port fuel injection (PFI) spark-ignition (SI) engine, mainly due to the use of a significantly higher compression ratio and overall lean combustion, coupled with unthrottled operation. However, sturdy structure, sophisticated high-pressure injection system, and complex aftertreatment for removing nitric oxides (NO_x) and particulate matter (PM) from exhaust stream contribute to the high cost of a diesel engine. This stimulates work on efficient gasoline engine technologies that could provide a more attractive trade-off for light passenger car vehicles. In short, intense research and development efforts are underway to develop an internal combustion engine that combines the best features of SI and DI engines. A critical step on the path toward increasing the fuel efficiency of a gasoline engine is the introduction of direct injection and development of the direct-injection spark-ignition (DISI) engine capable of part-load lean and unthrottled operation.

Since fuel is directly injected into the cylinder in DISI engines, the likelihood of fuel impingement on piston and cylinder surfaces is increasing. Many stratified DISI engines rely on the piston shape for directing fuel spray to the vicinity of the spark plug. Under these conditions, as well as in the case of unintentional fuel impingement during homogeneous DISI operation, fuel films can form on the piston top, with significant implications for combustion and emissions. Initially, researchers focused on spray impingement in diesel engines [1,2] and PFI engines [3]. More recently, experimental papers on high-pressure gasoline spray wall interactions [4–8] have pointed out that spray impingement in DISI engines must be studied in its own class because its fuel, spray structure, and injection pressure are different from those of DI and PFI engines.

The objective of this work is to advance the understanding of the fuel film behavior during the unintended fuel impingement for a homogeneous operating mode (early fuel injection during the intake stroke) in a wall-guided DISI engine under two different fuel injection timings (EOI 300 deg CA BTDC and EOI 270 deg CA BTDC). The analysis is based on detailed measurements of the instantaneous wall temperature using fast-response thermocouples. Analysis of measurements obtained simultaneously at different locations on the piston top allows determination of heat flux and assessment of the heat loss due to heating of the liquid fuel or its evaporation. Along with processing of the experimental information, computational fluid dynamics CFD calculations were carried out using boundary conditions from the experimental measurements. The role of CFD simulations is twofold. In the first step, the predictions are utilized to test the hypothesis that the fuel film evaporation happens quickly, and hence contributes to the heat loss detected on the metal surface below. Once this is established, the local fuel film thickness can be determined directly from measurements. Subsequently, the CFD predictions of fuel film dynamics can be validated at thermocouple locations, and

[1]Present address: Oak Ridge National Laboratory, Oak Ridge, TN.
[2]Present address: GM R&D Center, Warren, MI 48090-9055.

Contributed by the IC Engine Division of ASME for publication in the JOURNAL OF ENGINEERING FOR GAS TURBINES AND POWER. Manuscript received May 21, 2009; final manuscript revised September 4, 2009; published online April 19, 2010. Editor: Dilip R. Ballal.

Table 1 Engine specifications

Engine type	four-valve, single cylinder
Bore/stroke	86.0 mm/94.6 mm
Displacement	549.5 cm^3
Connecting rod length	152.2 mm
Compression ratio	11.0:1
IVO/IVC[a]	332 deg/620 deg[b]
EVO/EVC[c]	124 deg/386 deg[b]
Valve lift	10.0 mm
Injector	Swirl type (cone angle=53 deg)
Fuel type	Gasoline (H/C=1.92)

[a]Intake valve opening/intake valve closing.
[b]0 deg crank angle is assigned to TDC combustion.
[c]Exhaust valve opening/exhaust valve closing.

findings from experiments and CFD simulations can be combined to provide a complete insight into the fuel impingement, film formation, and evaporation.

This paper is organized as follows: The experimental setup is described in Sec. 2. Section 3 describes the methodology for local surface temperature and heat flux measurements. Section 5 begins with the instantaneous temperature and heat flux profiles measured on the piston top and the cylinder head for two different injection timings, showing the unintended fuel impingement for a homogeneous operating mode. CFD predictions of fuel film footprint and evaporation based on boundary conditions from the experimental measurements are shown in Sec. 5.2. Subsequently, the experimental findings are compared with CFD predictions in order to construct a complete picture about fuel film formation and dynamics. Section 6 offers a summary and conclusions.

2 Experimental Engine Setup

A modified single cylinder engine configured for DISI mixture preparation and combustion is used for engine dynamometer tests. A pent-roof shape cylinder head is designed especially for this experiment, but basic features correspond to a typical modern four-valve cylinder head. The engine specifications are summarized in Table 1.

The spark plug is located at the center of the cylinder head and the electrode length has been extended to 11 mm in order to facilitate stable combustion during stratified operation. A gasoline direct-injection fuel injector is located at the side between two intake valves. A deep-bowl piston was used to obtain a 11:1 compression ratio and assist in mixture preparation. The spray targeting and combustion chamber shape are typical of a wall-guided system with swirl charge motion. One of the intake ports has tangential orientation and is intended to produce an organized swirl motion, while the other contains a swirl control valve (SCV) installed approximately 180 mm upstream from the valve seat. Closing of the SCV controls the swirl/tumble intensity in the engine, and levels of in-cylinder swirl can be varied from 0.55 to 3.35. The exhaust gas was sampled at the exhaust plenum (approximately 55 cm from the exhaust valves) and analyzed to determine the total hydrocarbon (THC), nitric oxides (NO_x), carbon monoxide (CO), carbon dioxide (CO_2), and oxygen (O_2) concentrations.

The high-pressure fuel delivery system is based on a bladder-type accumulator. A bladder containing fuel is in a vessel pressurized by nitrogen (N_2). Regulating the pressure of N_2 allows control of the fuel injection pressure, which is 8.5 MPa in this study. A Kistler (Amherst, NY) 6125A piezoelectric pressure transducer measures the pressure trace in the cylinder with 0.5 deg crank angle resolution. A multislot flame arrestor is installed in front of the pressure transducer tip to minimize the effects of thermal shock on the pressure measurements and 50 consecutive cycles are recorded at any given condition. Top dead center (TDC) is determined by considering the thermodynamic loss angle. Detailed explanations of the experimental setup are given by Cho et al. [9,10].

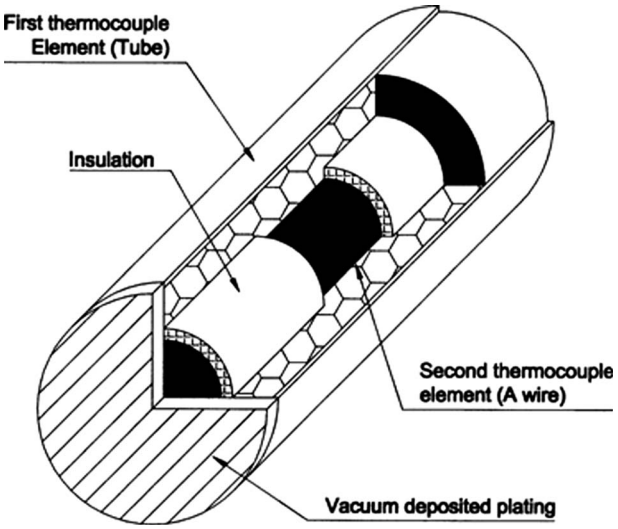

Fig. 1 Construction of coaxial thermocouple [11]

3 Temperature and Heat Flux Measurement

3.1 Methodology. Various surface thermocouple designs have been developed since Eichelberg's first attempt to measure instantaneous surface temperature in the combustion chamber in 1939 [11]. For our study, the instantaneous combustion chamber surface temperatures were measured by J-type coaxial fast-response thermocouples. The thermocouple consists of a thin wire of constantan coated with a ceramic insulation of high dielectric strength, swaged securely in a tube made of iron. A vacuum-deposited metallic plate forms a metallurgical bond with the two thermocouple elements, thus forming the thermocouple junction with $1-2$ μ thickness over the sensing end of the probe. The probes are custom-manufactured for engine experimentation and their response time is on the order of a microsecond [12]. Figure 1 is an illustration of the construction of a coaxial thermocouple. The sensing area at the tip is mounted flush with the combustion chamber surface.

As shown in Fig. 2(*a*), the signals of five thermocouple probes, including three probes in the piston bowl, and two probes in the cylinder head are used for this fuel impingement study. Measurement locations on the cylinder head are dictated by available space for installing special sleeves for mounting thermocouple probes. The probes on the cylinder head are located close to the periphery of the combustion chamber and their respective positions are denoted as "H1" and "H2" (Fig. 2(*a*)). The thermocouple signals on the cylinder head are routed directly outside the engine and joined with a reference junction at ambient temperature. In contrast, the thermocouple wires from the piston surface are routed to an isothermal plate installed on the inner surface of the piston skirt. In this case, a new reference junction is located at the isothermal plate and its temperature measured by a thermistor. This allows the use of highly durable stainless steel braided wire for transferring signals through the telemetry linkage and into the data acquisition system. A mechanical telemetry linkage system is used for conveying signals from the moving piston and connecting rod to the data acquisition system, as shown in Fig. 2(*b*). Detailed description of the fast-response thermocouples and telemetry linkage system are given by Cho et al. [9,10]

3.2 Instantaneous Heat Flux Calculation. The heat flux at the surface of the piston or combustion chamber is calculated by solving the unsteady heat conduction equation with two tempera-

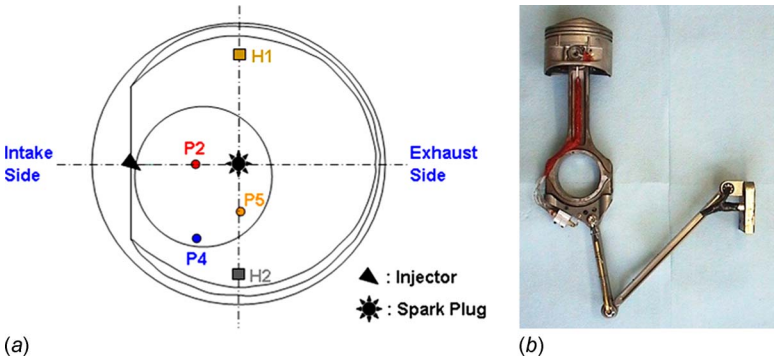

Fig. 2 Heat flux measurement instrumentation: (*a*) locations of thermocouple probes, and (*b*) mechanical telemetry linkage system

ture boundary conditions and one initial condition. Heat transfer is assumed to be one-dimensional, and normal to the wall surface. The solution of the unsteady heat conduction equation can be obtained by applying Fourier analysis, electrical analogy, or numerical finite difference method [13]. The Fourier analysis method was chosen in this study. The solution provides a time-dependent temperature variation at the surface, which is described as

$$T_w(t) = T_m + \sum_{n=1}^{N} [A_n \cos(n\omega t) + B_n \sin(n\omega t)] \quad (1)$$

where A_n and B_n are the Fourier coefficients, n is a harmonic number, ω is the angular frequency of the temperature cycle, and T_m is the time-averaged experimental surface temperature. A fast Fourier transform is applied to the measured surface temperature data to determine the Fourier coefficients A_n and B_n. Note that the selection of harmonic number n affects results significantly. In this study, the number of harmonic components required for high accuracy was $n=40$ [9]. Once coefficients A_n and B_n are determined, Fourier's law is applied to Eq. (1) to obtain the total heat flux. The total heat flux, which consists of a steady-state term and a time-dependent transient term, can be expressed as

$$q = \frac{k}{\delta}(T_m - T_\delta) + k\sum_{n=1}^{N} \varphi_n[(A_n + B_n)\cos(n\omega t) - (A_n - B_n)\sin(n\omega t)] \quad (2)$$

where $\varphi_n = \sqrt{(n\omega/2\alpha)}$, α is the thermal diffusivity of the wall material $(k/\rho c_p)$, and k, ρ, and c_p are thermal conductivity, density, and specific heat, respectively.

4 Computational Model

The CFD program used for this study was GMTEC, an in-house multidimensional modeling code developed at General Motors Research and Development [14]. GMTEC solves the unsteady equations of turbulent motion with chemically reactive ideal gases and couples them to the dynamics of vaporizing sprays. Solutions to the gas flow and spray liquid phase equations are found using a finite volume, arbitrary Lagrangian–Eulerian (ALE) method. The code solves the momentum, energy, and species conservation equations on unstructured grids and includes the capability to include nonconformal interfaces, which can also slide relative to each other. The liquid (dispersed) phase governing equations are solved in a Lagrangian fashion and are coupled to the gas phase via source terms. Computational parcels are used to represent a statistical collection of droplets with the same size, velocity, and temperature.

The computational mesh used for the GMTEC calculations is shown in Fig. 3. The 105,400 hexahedra cells accounted for the main and swirl ports, valves, and in-cylinder architecture (pent-roof and piston bowl). Turbulence was modeled using the standard k-ε model. The simulations were run for the entire intake and compression strokes in order to focus on mixture preparation (spray injection, atomization, vaporization, and wall impingement). The subsequent ignition and combustion processes were not modeled.

The injected gasoline fuel mass was divided among 20,000 computational parcels. A pressure-swirl injection model was included to simulate the sac and main spray development. The sac spray, which consisted of closely spaced liquid parcels having a small cone angle, was assumed to last for 0.085 ms. The transition from the sac spray to the main spray occurred over 0.1 ms, in which the outer cone angle increased linearly in time. The main spray was assumed to have a sheet thickness of 7.5 deg. The injected SMR of the main spray parcels was 28 μm distributed about a Rosin–Rammler distribution with parameter q_{rr} equal to 3.5.

Upon injection of the spray parcels, a series of models inherent in the CFD code were used to describe the dynamics of the spray and its interaction with the surrounding environment. Spray atomization was computed using the Taylor analogy breakup (TAB) model [15] with an adjusted C_k parameter set equal to 4.0. Droplet collision and coalescence was not modeled. Drop drag was simulated using the methodology of [16] which alters the drag coefficient of the parcels linearly with the distortion of the drop. Spray-wall impingement was modeled using the approach of [17] in conjunction with the splash criterion of Cossali et al. [18] and the modified energy dissipation model of Grover et al. [19,20]. The

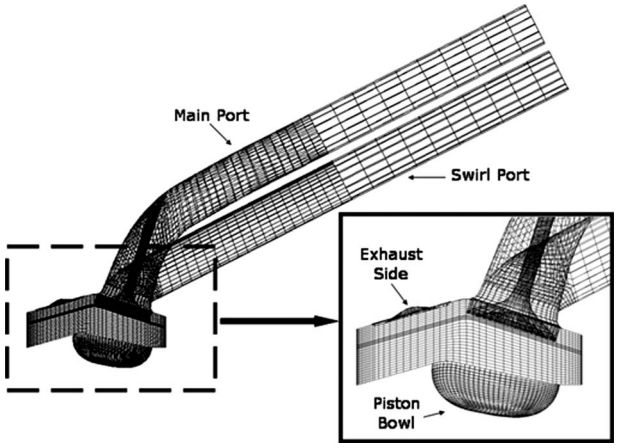

Fig. 3 Image of computational mesh used in GMTEC with close-up view of the engine cylinder. The grid consisted of 105,400 cells.

Table 2 Engine operating conditions and performance data

EOI	(deg CA BTDC)	300	270
Fuel flow rate	(mg/cycle)	12.2	12.3
A/F	-	14.7	14.6
Φ	-	0.99	1.00
MAP	(kPa)	46.6	45.4
EGR	(%)	15.8	14.2
$T_{\text{intake charge}}$	(°C)	94.2	94.7
T_{oil}	(°C)	89.4	88.9
T_{coolant}	(°C)	89.3	90.2
Spark timing	(deg CA BTDC)	22	22
Air swirl index	-	3.35	3.35
NMEP	(kPa)	290.9	289.2
COV of NMEP	-	1.17	0.92
$\eta_{\text{combustion}}$	(%)	94.0	93.4
T_{exhaust}	(°C)	663.2	665.1
EI NO	(g/kg fuel)	18.5	19.3
EI HC	(g/kg fuel)	22.7	22.7
PP	(bar)	19.9	20.2
LPP	(deg CA ATDC)	14.5	14.2

splash criterion treated droplet impact on dry surfaces with roughness or those with a pre-existing fuel puddle. The piston surface roughness was assumed to have a nominal value of 12 μm to account for combustion chamber deposits that may build during operation. The energy dissipation model was included to predict the loss of droplet energy prior to impact (i.e., kinetic and surface energies) due to collision with a surface. Droplet and fuel film vaporizations were modeled using in-house GM R&D models, which include multicomponent fuel effects, following the approach of Lippert and Reitz [21]. The composition of gasoline was assumed to follow a Γ-distribution for molecular weight, having a mean of 107 with α, β, and γ equal to 8.755, 11, and 0, respectively.

5 Results and Discussion

5.1 Experimental Measurements. Two different engine test conditions at 2000 rpm, one with advanced injection timing EOI 300 deg CA BTDC (SOI 318 deg CA BTDC) and other with retarded injection timing EOI 270 deg CA BTDC (SOI 288 deg CA BTDC), have been run to understand the formation, transport, and vaporization of a wall fuel film located on the piston surface under homogeneous operating mode. Detailed information about the operating conditions and performance data are shown in Table 2.

Figure 4 shows the comparison of 50-cycle averaged wall temperature histories between the two cases. Corresponding heat flux histories for the two different fuel injection timings are shown in Figs. 5(*a*) and 5(*b*). A noticeable difference is observed between the two cases: a rapid wall temperature decrease at the piston (P2, P4, and P5) is detected right after SOI timing in the advanced injection case, while no wall temperature fluctuation is found in the retarded injection case. A rapid wall temperature decrease is not detected at the cylinder head in any of the two cases. A negative heat flux fluctuation due to rapid wall temperature decrease is observed in the advanced injection case, but the heat flux histories for the retarded injection case does not show any negative heat flux excursions. This rapid decrease in temperature and negative heat flux fluctuation can be explained by the fuel impingement at the piston surface.

Figure 6 shows the schematic view of the piston locations relative to the fire deck at two different injection timings: the distance from the fire deck to the top surface of the piston at the time of SOI 318 deg CA BTDC (advanced injection case) is 15.3 mm, and that of SOI 288 deg CA BTDC (retarded injection case) is 34.2 mm. This piston location difference between the two timings

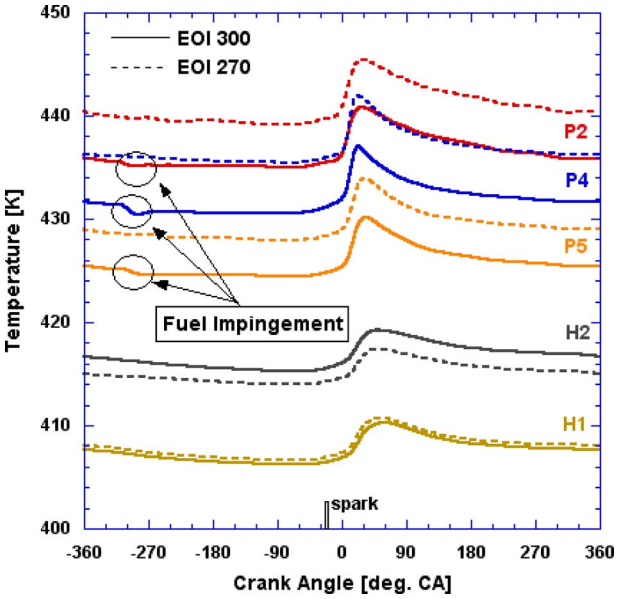

Fig. 4 Comparison of 50-cycle averaged surface temperature histories for EOI 300 and EOI 270 deg CA BTDC cases at 2000 rpm, homogeneous mode

(18.9 mm) is a main factor influencing fuel impingement on the piston top. As seen in Fig. 4, the overall wall temperature levels at the piston in the advanced injection case are lower than in the retarded injection case due to the piston cooling by fuel impingement. No significant wall temperature difference at the cylinder head is observed in both cases.

In summary, the fast-response thermocouples are sensitive enough to pick up the effects of fuel impingement. Local surface temperature measurements can be used to support CFD predictions by providing the boundary conditions and indication of spatial variations. In turn, CFD will provide a critical piece of information for determining the mass of fuel film from heat flux measurements, namely, an indication whether both fuel heating and evaporation (full or partial) have to be taken into account. The combination of the CFD predictions and quantitative analysis of heat flux measurements can construct a complete picture of the fuel film phenomena, i.e., fuel film footprint and spatial variations in film thickness, and total mass of impinged fuel at the piston surface.

5.2 Results of CFD Predictions. The CFD calculations were performed for both injection timings. The initial conditions of the code are based on the experimental measurements and are given in Table 3. Figures 7 and 8 show the snapshots of (a) fuel film thickness and its distribution and (b) the injected fuel history of CFD predictions for EOI 300 deg CA BTDC and EOI 270 deg CA BTDC cases, respectively. Predictions for EOI 300 deg CA BTDC indicate significant fuel impingement at locations P2 and P4, but no fuel impingement at location P5. However, the CFD calculation for the EOI 270 deg CA BTDC case indicates only a very small amount of fuel film at location P5, and negligible impingement at the other two locations.

Figure 7 shows more fuel impingement at the location P4 than P2. Thicker fuel film at the location P4 is predicted by CFD. The maximum fuel film thicknesses at each location were observed at 290 deg CA BTDC: approximately 0.8 μm at location P3, approximately 1.2 μm at location P4, and 0 μm at location P5. The injected fuel history diagrams, as shown in Figs. 7(*b*) and 8(*b*), indicate that the mass of liquid fuel at the wall in the retarded injection timing case (EOI 270 deg CA BTDC) is roughly 1/3 of the mass of liquid at the wall in the advanced injection timing case (EOI 300 deg CA BTDC). Due to film dynamics, the fuel film

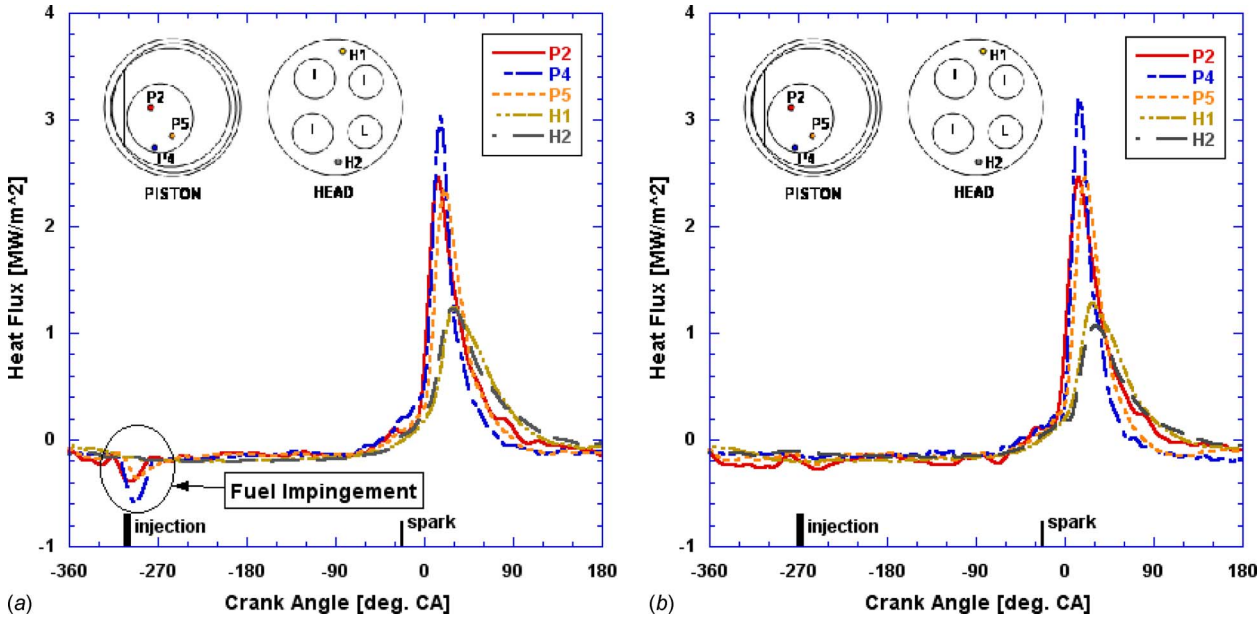

Fig. 5 50-cycle averaged heat flux histories (*a*) for advanced injection timing (EOI 300 deg CA BTDC) and (*b*) for retarded injection timing (EOI 270 deg CA BTDC) at 2000 rpm, homogeneous mode

thickness in the retarded injection timing case is an order of magnitude less than that in the advanced injection timing case. Based on these observations, the film mass estimation technique will be applied to the advanced injection timing case (EOI 300 deg CA BTDC), and hence the rest of the results in the paper pertain to that case.

The computed vaporization history of injected fuel and the measured heat flux history during the same crank angle period are shown in Fig. 9. The total injected mass of fuel is 12.21 mg/cycle, and about 60% of the mass of fuel injected is evaporated by EOI

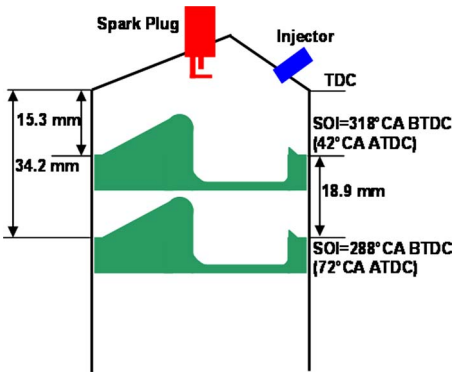

Fig. 6 Schematic view of piston location for both injection timings

Table 3 Initial conditions of CFD code

EOI	(deg CA BTDC)	300	270
MAP	(kPa)	46.6	45.4
T_{intake}	(°C)	94.0	94.7
T_{piston}	(°C)	157.5	160.8
T_{head}	(°C)	139.0	138.0
T_{linear}	(°C)	129.0	128.0
Air swirl index	-	3.35	3.35
Mass of fuel injected	(mg/cycle)	12.21	12.28
SOI	(deg CA BTDC)	318	288

(300 deg CA BTDC). The predicted overall vaporization rate seems to be faster than some past studies, which reported that about 40% of the total mass of injected fuel is evaporated by EOI [22,23]. Our CFD predictions show that the mass of fuel vapor from the wall reaches a constant value around 270 deg CA BTDC. At that instant, the predicted mass of vapor from the fuel film reaches 2.72 mg and the mass of liquid fuel at the wall is 0.08 mg. Thus, the total mass of fuel that has impinged the wall predicted with CFD becomes 2.8 mg. In other words, about 23% of the injected fuel mass reaches the piston surface. The measured heat flux histories indicate that the negative heat flux fluctuations at each location end at about 270 deg CA BTDC, as shown in Fig. 9(*b*). The CFD results depicted in Fig. 9(*a*) indicate that most of the injected fuel evaporated during the time interval of measured negative heat flux fluctuation. Hence, the fuel starts to evaporate immediately after the fuel impinges on the piston surface, with no time delay observed. About 97% of the fuel film at the piston surface evaporated by 270 deg CA BTDC; hence, the evaporation process should be considered in the quantitative analysis of experimental measurements. In summary, the negative heat flux at the piston surface is due to the combined effect of heating up the liquid fuel and its evaporation.

5.3 Quantitative Analysis of Experimental Results. The assumptions applied to the analysis of fuel film mass estimation are as follows: commercial gasoline properties, with same values as in the CFD calculations, are used in this analysis, i.e., specific heat c_p=2.2 kJ/kg K, heat of vaporization h_{fg}=369 kJ/kg, and density of liquid fuel ρ=751 kg/m^3. The initial liquid fuel temperature is assumed to be the same as the engine coolant temperature, or 89°C. The piston wall temperatures at each location are prescribed to be the average values of measured piston wall temperatures during the negative heat flux fluctuation period: 162.1°C at location P2, 157.6°C at location P4, and 151.6°C at location P5. The CFD calculation provided the crank angle resolved fuel film wetted area, as shown in Fig. 10, since this information could not be obtained from measurements. The equivalent fuel film wetted area is assumed to be the average area during the interval defined by the negative heat flux fluctuation period (22.14 cm^2) and to be equally distributed among the three heat flux probe locations (P2,

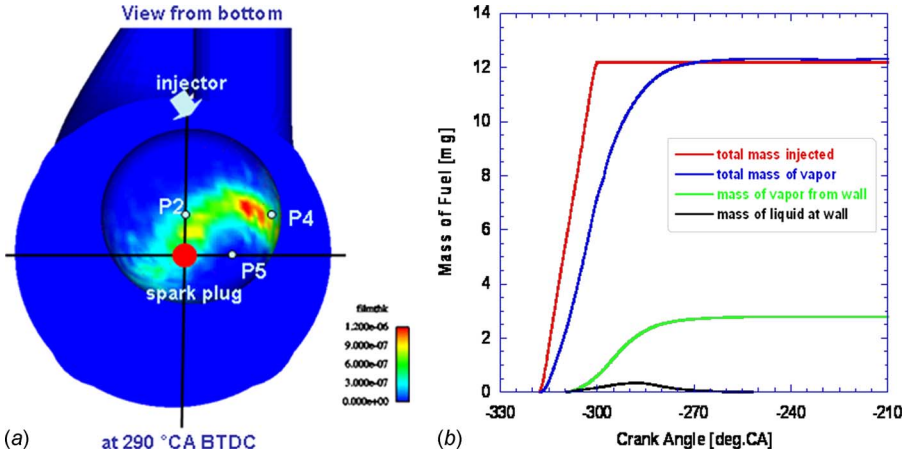

Fig. 7 CFD predictions for advanced injection timing case (EOI 300 deg CA BTDC): (*a*) snap shots of the fuel film thickness and its distribution, and (*b*) injected fuel history

P4, and P5). The film area observed in Fig. 10 after 270 deg CA BTDC is not relevant since the fuel film thickness becomes negligible after that point.

In order to quantify the heat loss due to fuel impingement, the start and end of calculation timings at each heat flux probe location are determined by taking the derivatives of heat flux histories. The start and end of calculation timings are defined as the times when the sign of the first derivatives of the heat fluxes changes from positive to negative. Table 4 shows the timings of the start and end of calculation at each location.

After determining the start and end of calculations, the negative heat flux fluctuation during that window can be integrated to obtain the gross heat loss per unit area due to fuel impingement, which is represented by the sum of "hatched" and "gridded" colored areas in Fig. 11, as

$$\frac{\text{Gross heat loss}}{\text{Area}} = \int_{\text{start of calculation}}^{\text{end of calculation}} Q''(\theta)d\theta \tag{3}$$

To quantify the net amount of heat loss per area due to fuel impingement, the nonparticipating heat loss per area, which is represented by "gridded" area in Fig. 11, should be subtracted from the gross heat loss per area

$$\frac{\text{Net heat loss}}{\text{Area}} = (\text{Gross} - \text{Nonparticipating})\frac{\text{Heat loss}}{\text{Area}} \tag{4}$$

By multiplying the estimated net heat loss per area with the fuel film wetted area from the CFD calculations, the net heat loss due to fuel impingement is determined at each heat flux probe location, as summarized in Table 5.

Based on the guidance from the CFD work, the evaporation of fuel at the piston surface should be considered during the measured negative heat flux fluctuation period. In other words, the amount of calculated net heat loss during fuel impingement is due to both heating up and vaporizing the fuel, i.e.

$$Q = m_{\text{film}} \times c_p \times (T_{\text{wall}} - T_{\text{fuel}}) + C \times m_{\text{film}} \times h_{\text{fg}} \tag{5}$$

$$m_{\text{film}} = m_{\text{liquid}} + m_{\text{vapor}} \tag{6}$$

$$m_{\text{vapor}} = C \times m_{\text{film}} \tag{7}$$

$$m_{\text{liquid}} = (1 - C) \times m_{\text{film}} \tag{8}$$

The first term at the right hand side of Eq. (5) represents the heat used for heating up the fuel, while the second term represents the heat needed for vaporizing the fuel. Varying the value of the evaporated fraction of the fuel C, the mass of fuel film m_{film},

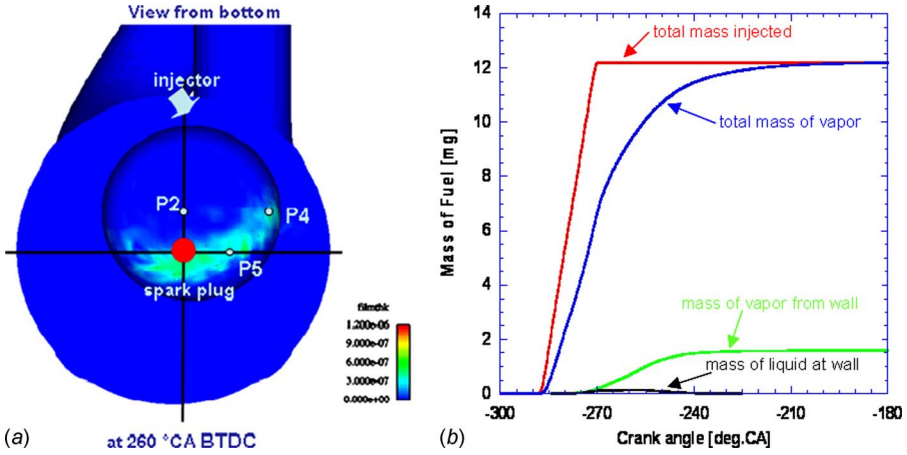

Fig. 8 CFD predictions for retarded injection timing case (EOI 270 deg CA BTDC): (*a*) snap shots of the fuel film thickness and its distribution, and (*b*) injected fuel history

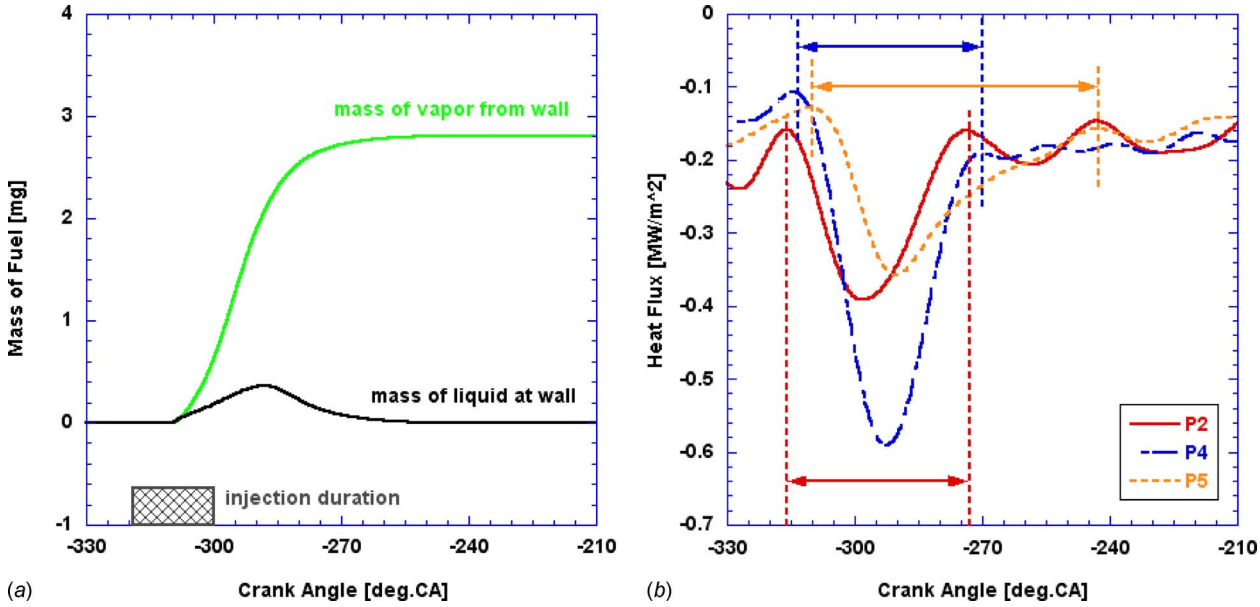

Fig. 9 (*a*) CFD predictions of vaporization history of injected fuel; (*b*) measurements of the local heat flux due to fuel film warmup and evaporation for EOI 300 deg CA BTDC

which is the only unknown in Eq. (5), could be estimated. The mass of vapor m_{vapor} and liquid m_{liquid} could be quantified after the mass of fuel film m_{film} is evaluated using Eqs. (7) and (8), respectively.

Table 6 shows estimates of fuel film mass based on the experimental heat flux measurements. For one extreme, assuming that the heat loss on the piston surface is only due to heating up the fuel ($C=0$) yields an unrealistically high value for the fuel film mass ($m_{film}=m_{liquid}=7.9$ mg). For the other extreme, assuming that the heat loss is due to both heating up the fuel and its complete evaporation ($C=1$) yields the mass of fuel film of 2.4 mg. The latter is in good agreement with the CFD prediction of 2.80 mg. Therefore, we confirm that the heat loss from the piston surface occurring during the negative heat flux period is due to heating up the liquid fuel and its complete evaporation. The fast evaporation rates of injected fuel either from upstream or at the piston surface can be explained by the very low manifold pressure

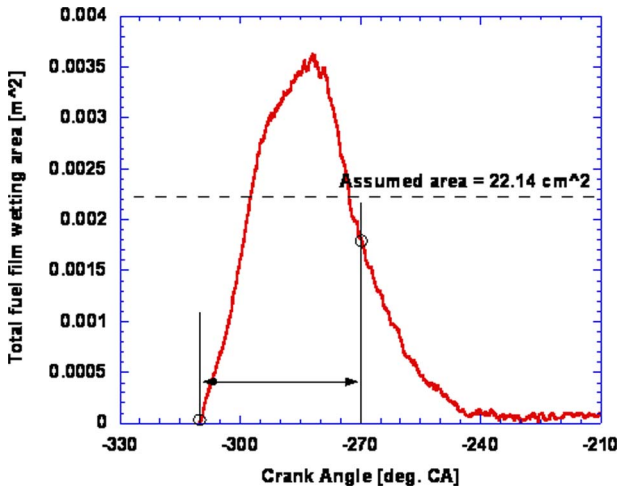

Fig. 10 Predicted crank angle resolved fuel film wetted area for advanced injection timing case (EOI 300 deg CA BTDC case)

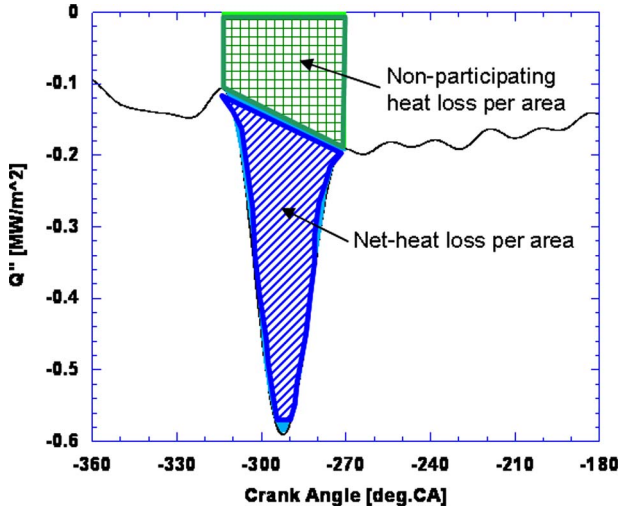

Fig. 11 Heat loss per area due to fuel impingement

Table 4 Start/end of the heat loss calculation

Locations	Start of calculation (deg CA BTDC)	End of calculation (deg CA BTDC)
P2	316.0	273.5
P4	314.5	270.0
P5	310.5	242.5

Table 5 Results of calculated net heat loss

Location	Net heat loss (J)
P2	0.325
P4	0.571
P5	0.387
Total	1.283

Table 6 Results of mass of fuel film from the experimental measurements (unit: mg)

	P2			P4			P5			Total		
C	m_{vapor}	m_{liquid}	m_{film}	m_{vapor}	m_{liquid}	m_{film}	m_{vapor}	m_{liquid}	m_{film}	m_{vapor}	m_{liquid}	m_{film}
0.0	0.00	2.02	2.02	0.00	3.55	3.55	0.00	2.41	2.41	0.00	7.98	7.98
0.1	0.16	1.48	1.64	0.29	2.60	2.89	0.20	1.76	1.96	0.65	5.84	6.49
0.2	0.28	1.11	1.38	0.49	1.95	2.43	0.33	1.32	1.65	1.09	4.38	5.47
0.3	0.36	0.84	1.20	0.63	1.47	2.10	0.43	1.00	1.43	1.42	3.31	4.73
0.4	0.42	0.63	1.05	0.74	1.11	1.85	0.50	0.75	1.26	1.66	2.50	4.16
0.5	0.47	0.47	0.94	0.83	0.83	1.65	0.56	0.56	1.12	1.86	1.86	3.72
0.6	0.51	0.34	0.85	0.90	0.60	1.49	0.61	0.41	1.01	2.01	1.34	3.36
0.7	0.54	0.23	0.77	0.95	0.41	1.36	0.65	0.28	0.92	2.14	0.92	3.06
0.8	0.57	0.14	0.71	1.00	0.25	1.25	0.68	0.17	0.85	2.25	0.56	2.81
0.9	0.59	0.07	0.66	1.04	0.12	1.16	0.71	0.08	0.79	2.34	0.26	2.60
1.0	0.61	0.00	0.61	1.08	0.00	1.08	0.73	0.00	0.73	2.42	0.00	2.42

(46.6 kPa), and hence cylinder pressure at this operating condition. The qualitative comparison of the local heat loss calculated from the experimental measurements and the local fuel film thickness from the CFD predictions indicates a correct trend for locations P2 and P4, as shown in Table 5. However, the experimental measurement indicates the presence of fuel at location P5, while the fuel film footprint from the CFD calculations does not cover that location. This could be due to the variations in the practical injector or the effect of sac spray, since P5 is aligned with the spray axis.

6 Conclusions

In-cylinder heat transfer measurements and CFD fuel spray simulation have been combined to study the fuel impingement on the piston top of a homogeneous DISI engine. The piston surface was instrumented with fast-response thermocouples to provide instantaneous surface temperature measurements at multiple locations on the piston top. Negative swings of the instantaneous surface temperature were observed at three locations during early injection (SOI 42 deg CA after TDC intake), thus confirming the ability of the thermocouples to capture the effects of impingement. Retarding injection timing by 30 deg eliminated the effect of fuel impingement. Heat flux analysis using the instantaneous temperature signal provides information about the heat loss due to liquid film heating/evaporation. The full quantitative analysis of the fuel film mass and thickness depended on the hypothesis pertaining to the rate of evaporation, and this was tested with a companion CFD study.

The experimental information established boundary conditions for setting up CFD calculations. The predictions of the CFD code with advanced models for spray atomization, impingement, and splash indicate very fast rate of fuel evaporation from the piston surface under conditions studied in this work, i.e., throttled part-load operation with homogenous mixture. This enables calculations of fuel film mass from measurements, since the heat loss measured on the surface can be tied directly to the heating of the fuel film and its complete evaporation. The wetted area is estimated based on CFD predictions.

The total mass of fuel film resulting from the spray impingement determined from measurements is in good agreement with the CFD prediction (2.42 mg versus 2.8 mg). This means that 23% of the fuel injected impinges upon the piston and creates a fuel film with thickness of up to 1.2 μm. The simulated fuel film thickness and transport corroborate well temporally and spatially with heat flux measurements at two out of three locations, which are directly in the path of the spray. The measurements indicated the presence of fuel at the third location as well, although this was not indicted by CFD. The likely reason for the discrepancy is the imperfection of the real injector and the presence of the sac spray. In summary, a synergistic methodology combining heat flux measurements with CFD provides complete and unique insight into the complex spray development and impingement phenomena. The power of the techniques stems from the fact that the experimental analysis and the CFD work complement each other in a way that not only increases the amount of information available, but also elevates the level of confidence in the findings.

Acknowledgment

This research has been sponsored by the General Motors/University of Michigan Collaborative Research Laboratory for Engine System Research at the University of Michigan.

Nomenclature

A_n, B_n = Fourier coefficients
A/F = air-fuel ratio
BTDC = before top dead center
C = constant
COV = coefficient of variance
c_p = specific heat
EGR = exhaust gas recirculation
EI = emission index
EOI = end of injection
h_{fg} = heat of vaporization
LPP = location of peak cylinder pressure
MAP = manifold absolute pressure
m_{film} = mass of fuel film
m_{liquid} = mass of liquid fuel
m_{vapor} = mass of vapor fuel
n, N = harmonic number
NMEP = net mean effective pressure
PP = peak cylinder pressure
SMR = Sauter mean radius
SOI = start of injection
T = temperature
T_{head} = cylinder head surface temperature
T_{intake} = intake charge temperature
T_{linear} = liner surface temperature
T_m = time-averaged temperature
T_{piston} = piston surface temperature
T_δ = temperature at a distance δ from surface
α = thermal diffusivity
Φ = equivalence ratio
η = efficiency
κ = thermal conductivity
ρ = density
ω = angular frequency

References

[1] Naber, J., and Reitz, R. D., 1988, "Modeling Engine Spray/Wall Impingement," SAE Paper No. 880107.

[2] Naber, J., and Farrel, P. V., 1993, "Hydrodynamics of Droplet Impingement on a Heat Surface," SAE Paper No. 930919.
[3] Senda, J., Ohnishi, M., Takahashi, T., Fujimoto, H., Utsunomiya, A., and Wakatabe, M., 1999, "Measurement and Modeling on Wall Wetted Fuel Film Profile and Mixture Preparation in Intake Manifold for SI Engine," SAE Paper No. 1999-01-0799.
[4] Yoo, J., Kim, S., Zhao, F. Q., Lai, M. C., and Lee, K., 1998, "Characterization of Direct Injection Gasoline Sprays in Different Ambient and Wall Impingement Conditions," SAE Paper No. 982702.
[5] Stevens, E., and Steeper, R., 2001, "Piston Wetting in an Optical DISI Engine: Fuel Films, Pool Fires, and Soot Generation," SAE Paper No. 2001-01-1203.
[6] Karlsson, R. B., and Heywood, J. B., 2001, "Piston Fuel Film Observations in an Optical Access GDI Engine," SAE Paper No. 2001-01-2022.
[7] Hennessey, R., Fuentes, A., and Wicker, R., 2001, "Effect of Injection Timing on Piston Surface Fuel Impingement and Vaporization in Direct injection, Spark Ignition Engines," SAE Paper No. 2001-01-2025.
[8] Drake, M. C., Fansler, T. D., Solomon, A. S., and Szekely, G. A., 2000, "Piston Fuel Films as a Source of Smoke and Hydrocarbon Emissions From a Wall-Controlled Spark-Ignited Direct-Injection Engine," SAE Paper No. 2003-01-0547.
[9] Cho, K., 2003, "Characterization of Combustion and Heat Transfer in a Direct Injection Spark Ignition Engine Through Measurements of Instantaneous Combustion Chamber Surface Temperature," Ph.D. thesis, University of Michigan, Ann Arbor, MI.
[10] Cho, K., Assanis, D., Filipi, Z., Szekely, G., Najt, P., and Rask, R., 2008, "Experimental Investigation of Combustion and Heat transfer in a Direct-Injection Spark Ignition Engine via Instantaneous Combustion Chamber Surface Temperature Measurements," Proc. Inst. Mech. Eng., Part D (J. Automobile Eng.), **222**, pp. 2219–2233.
[11] Eichelberg, G., 1939, "Some New Investigations on Old Combustion-Engine Problems," Engineering, **148**, pp. 463–466 and 547–560.
[12] Medtherm Corporation, 2000, *Medtherm Corporation Bulletin 500*, Medtherm, Huntsville, AL.
[13] Borman, G., and Nishiwaki, K., 1987, "Internal-Combustion Engine Heat Transfer," Prog. Energy Combust. Sci., **13**, pp. 1–46.
[14] Khalighi, B., El Tary, S. H., Haworth, D. C., and Huebler, M. S., 1995, "Computation and Measurement of Flow and Combustion in a Four-Valve Engine With Intake Variations," SAE Paper No. 950287.
[15] O'Rourke, P. J., and Amsden, A. A., 1987, "The Tab Method for Numerical Calculation of Spray Breakup," SAE Paper No. 872089.
[16] Liu, A. B., Mather, D., and Reitz, R. D., 1993, "Modeling the Effects of Drop Drag and Breakup on Fuel Sprays," SAE Paper No. 930072.
[17] Stanton, D., and Rutland, C., 1996, "Modeling Fuel Film Formation and Wall Interaction in Diesel Engines," SAE Paper No. 960628.
[18] Cossali, G., Coghe, A., and Marengo, M., 1997, "The Impact of a Single Drop on a Wetted Solid Surface," Exp. Fluids, **22**, pp. 463–472.
[19] Grover, R. O., and Assanis, D., 2001, "A Spray Wall Impingement Model Based Upon Conservation Principles," Fifth International Symposium on Diagnostics and Modeling of Combustion in Internal Combustion Engines, pp. 551–559.
[20] Grover, R. O., Lippert, A. M., Assanis, D. N., El Tahry, S., Drake, M., Fansler, T., and Harrington, D., 2002, "A Critical Analysis of Splash Criteria for GDI Spray Impingement," 15th Annual Conference on Liquid Atomization and Spray Systems, Madison, WI, May 14–17, pp. 93–97.
[21] Lippert, A. M., and Reitz, R. D., 1997, "Modeling of Multi-component Fuels Continuous Distributions With Application to Droplet Evaporation and Sprays," SAE Paper No. 972882.
[22] Han, Z., Fan, L., and Reitz, R. D., 1997, "Multidimensional Modeling of Spray Atomization and Air-Fuel Mixing in a Direct-Injection Spark-Ignition Engine," SAE Paper No. 970884.
[23] Glaspie, C. R., Jaye, J. R., Lawrence, T. G., Lounsberry, T. H., Mann, L. B., Opra, J. J., Roth, D. B., and Zhao, F.-Q., 1999, "Application of Design and Development Techniques for Direct Injection Spark Ignition Engines," SAE Paper No. 1999-01-0506.